Published in final edited form as:
*Biomaterials*. 2011 May ; 32(13): 3395–3403. doi:10.1016/j.biomaterials.2011.01.029.

# The effects of combined micron-/submicron-scale surface roughness and nanoscale features on cell proliferation and differentiation

**Rolando A. Gittens I**[1,2], **Taylor McLachlan**[1], **Ye Cai**[1], **Simon Berner**[3], **Rina Tannenbaum**[1], **Zvi Schwartz**[2,5], **Kenneth H. Sandhage**[1,2,4], and **Barbara D. Boyan**[1,2,5]

[1]School of Materials Science and Engineering, Georgia Institute of Technology, Atlanta, Georgia, USA [2]Institute for Bioengineering and Bioscience, Georgia Institute of Technology, Atlanta, Georgia, USA [3]Institut Straumann AG, Basel, Switzerland [4]School of Chemistry and Biochemistry, Georgia Institute of Technology, Atlanta, Georgia, USA [5]Wallace H. Coulter Department of Biomedical Engineering at Georgia Tech and Emory University, Georgia Institute of Technology, Atlanta, GA, USA

## Abstract

Titanium (Ti) osseointegration is critical for the success of dental and orthopaedic implants. Previous studies have shown that surface roughness at the micro- and submicro-scales promotes osseointegration by enhancing osteoblast differentiation and local factor production. Only relatively recently have the effects of nanoscale roughness on cell response been considered. The aim of the present study was to develop a simple and scalable surface modification treatment that introduces nanoscale features to the surfaces of Ti substrates without greatly affecting other surface features, and to determine the effects of such superimposed nano-features on the differentiation and local factor production of osteoblasts. A simple oxidation treatment was developed for generating controlled nanoscale topographies on Ti surfaces, while retaining the starting micro-/submicro-scale roughness. Such nano-modified surfaces also possessed similar elemental compositions, and exhibited similar contact angles, as the original surfaces, but possessed a different surface crystal structure. MG63 cells were seeded on machined (PT), nano-modified PT (NMPT), sandblasted/acid-etched (SLA), and nano-modified SLA (NMSLA) Ti disks. The results suggested that the introduction of such nanoscale structures in combination with micro-/submicro-scale roughness improves osteoblast differentiation and local factor production, which, in turn, indicates the potential for improved implant osseointegration *in vivo*.

### Keywords

(4 to 6) nanotopography; titanium oxide; surface roughness; titanium; bone; implant; osteoblasts



**Address for Correspondence:** Barbara D. Boyan, Ph.D., Institute for Bioengineering and Bioscience, 315 Ferst Drive NW, Georgia Institute of Technology, Atlanta, GA 30332-0363, Phone: 404-385-4108, FAX: 404-894-2291, barbara.boyan@bme.gatech.edu.

## 1. Introduction

Integration of titanium (Ti) implants with the surrounding bone is critical for successful bone regeneration and healing in dental and orthopedic applications. The desire to accelerate and improve osseointegration drives many implantology research and development efforts, particularly for patients whose bones have been compromised by disease or age. Previous work has shown that the surface characteristics of implants have a direct influence on tissue response by affecting protein adsorption and by modulating cell proliferation and differentiation [1–2]. Surface characteristics such as roughness [3–4], chemistry [5–7] and energy [8–9] have been reported to significantly influence cell differentiation, local factor production and, consequently, bone growth and osseointegration [10–11].

Surface modification strategies for metallic implants to improve osseointegration have attempted to mimic the characteristics of bone [12–15]. During bone remodeling, previously-formed bone is resorbed by osteoclasts, in part to remove micro-cracks before new bone is formed in these primed regions [16–17]. Resorption lacunae left by osteoclasts, created through acidification and proteinase activity [18], have a distinct hierarchical structural complexity [19–20]. Resorption lacunae consist of microscale pits (up to 100 μm in diameter and 50 μm in depth [21–23]) with submicro-scale roughness formed by the irregular acid-etching at the ruffled border of the osteoclast [18–19] and nanoscale features created by the collagen fibers left on the surface [20, 22].

Several studies have shown that increases in surface micro- and submicro-scale roughness, with feature sizes comparable to those of resorption pits and cell dimensions, lead to enhanced osteoblast differentiation and local factor production *in vitro* [24–25], increased bone-to-implant contact *in vivo* [26–27] and improved clinical rates of wound healing [28–29]. Surface nanoscale roughness, which directly corresponds to the sizes of proteins and cell membrane receptors, could also play an important role in osteoblast differentiation and tissue regeneration (Fig. 1).

The effect of nanoscale surface roughness on osteoblast response has drawn the attention of several research groups over the last decade [30–33]. The literature on this topic is dominated by studies on the initial interactions between osteoblasts and nano-modified polymeric substrates, and such work has indicated that nanoscale roughness can significantly affect cell adhesion [34], proliferation [35], and spreading [36]. Similar results have been found for ceramic [37] and metallic [38] substrates. However, other studies report either a decrease in osteoblast proliferation with an increase in nanoscale roughness [39], or no effect of nanoscale roughness on proliferation [40] in the absence of microscale surface roughness [12, 41].

Relatively few studies have examined the effects of nanostructured surfaces on osteoblast differentiation [12, 36–37, 42–43]. Some reports have indicated that increased osteoblast proliferation on nanostructured surfaces coincided with an increase in alkaline phosphatase (ALP) synthesis, increased Ca-containing mineral deposition [37], and higher immunostaining of osteocalcin (OCN) and osteopontin [36]. Gene expression studies have shown an increase in the expression of RUNX2, osterix (OSX), and bone sialoprotein (BSP) in osteoblasts grown on nano-roughened surfaces [42–43]. Two studies [12, 41] examined the protein levels of different differentiation markers and local factors, and both of these studies reported an increase in differentiation, and an increase in factors $PGE_2$ and active TGF-β1, when submicro- to nanoscale roughness was introduced to micro-rough substrates.

More recent studies have focused on the hierarchical combination of both micro- and nanoscale roughness to promote osseointegration on clinically-relevant surfaces [12–14, 44–45]. Although some of these studies have reported promising results of increased osteoblast

proliferation and differentiation, it has been challenging to create a tailored hierarchical surface without altering other underlying characteristics of the substrate (particularly the microscale roughness and surface chemistry) [13–14, 45]. For this reason, it has been difficult to decouple the effects of nanoscale features from those of other surface features, such as surface micro-roughness, surface chemistry, and/or surface energy. Additionally, the simultaneous increase in osteoblast proliferation and differentiation caused by nanoscale roughness remains controversial due to some contradictory results [39–40, 44], which may have been influenced by differences in the types of cells and in the types of nanoscale surface modifications used in these experiments.

The objectives of the present study were twofold. First, we aimed to develop a simple and scalable oxidation-induced surface modification process of clinical relevance in order to alter the nanoscale topography of Ti substrates without greatly affecting surface chemistry or the starting micro-/submicro-scale roughness. Second, we aimed to evaluate the influence of such modified nanoscale surface topography, with and without additional micro-/submicro-scale roughness, *in vitro* on the differentiation and local factor production of human osteoblast-like MG63 cells.

## 2. Materials and Methods

### 2.1 Titanium disks

Ti disks with a diameter of 15 mm were punched from 1 mm thick sheets of grade 2 unalloyed Ti (ASTM F67 unalloyed Ti for surgical implant applications) and supplied by Institut Straumann AG (Basel, Switzerland). After degreasing the disks in acetone, the disks were exposed at 55°C for 30 seconds to an aqueous solution consisting of 2% ammonium fluoride, 2% hydrofluoric acid and 10% nitric acid to generate “pre-treated” (PT) Ti disks. The PT disks were further sandblasted with corundum grit (0.25–0.50 μm) at 5 bar, followed by etching in a solution of hydrochloric and sulfuric acids heated above 100°C for several minutes (proprietary process of Institut Straumann AG) to produce “sandblasted-large-grit-acid-etched” (SLA) disks. The samples were then rinsed with water and sterilized by gamma irradiation at 25 kGy overnight (> 12 h).

### 2.2 Surface modification

A simple and scalable process for achieving a homogenous and relatively high surface density of nanoscale structures on titanium metal surfaces, referred to herein as “nanoscale modification” (NM), was developed [46]. An additional attribute of the surface modification process is that it does not require a straight line path to modify or superimpose the nanoscale structures on the surface (non-line-of-sight). All PT and SLA disks were cleaned and sterilized before and after the NM treatment process. Prior to NM treatment, samples were cleaned using a protocol that involved two 15 minute sonication cycles each in detergent, ultra-pure water, acetone, isopropanol, ethanol, and then three 10 minute sonication cycles each in ultrapure water, followed by plasma cleaning for 2 minutes at a maximum oxygen pressure of 0.27 mbar and at an RF power of 6.8 W (PDC-32G plasma cleaner, Harrick Plasma, Ithaca, NY). The NM treatments consisted of exposure of the cleaned specimens at 740°C to flowing (0.85 standard liters per minute) synthetic air (21% $O_2$, 79% $N_2$) at 1 atm for varied times. To evaluate the change in surface topography with exposure time, PT samples were treated for 45 minutes (NMPT45), 90 minutes (NMPT90), and 180 minutes (NMPT180). The development of nanoscale features on specimen surfaces was evaluated using scanning electron microscopy (SEM). The mass increase of the samples during such NM treatment was monitored via thermogravimetric (TG) analysis (Q50, TA Instruments, New Castle, DE). After optimization of the NM treatment using PT samples, this treatment was applied to SLA samples. Prior to use in cell experiments, the NM-treated PT (NMPT)

and NM-treated SLA (NMSLA) samples, and their respective unmodified controls, were cleaned by sonication in detergent and ultra-pure water and autoclave sterilized.

### 2.3 Surface characterization

The NMPT and NMSLA specimens were examined after sterilization by a variety of surface-sensitive techniques as described below.

**2.3.1 Scanning electron microscopy (SEM)—**The specimen surface topography was qualitatively evaluated using a field-emission-gun scanning electron microscope (Ultra 60 FEG-SEM, Carl Zeiss SMT Ltd., Cambridge, UK). Images were recorded using a 5 kV accelerating voltage and 30 μm aperture. Image analysis software (ImageJ, NIH software) was used to evaluate the dimensions of nanoscale structural features generated by the NM treatment.

**2.3.2 Transmission electron microscopy (TEM)—**The thickness and crystal structure of the oxide layer formed upon NM treatment was evaluated using a field-emission-gun transmission electron microscope (HF-2000 FEG-TEM, Hitachi High Technologies America, Inc., Pleasanton, CA). The NMPT90 sample was embedded in epoxy, cross-sectioned, and then ground, polished, dimpled, and ion-milled to perforation. TEM characterization was then performed using an accelerating voltage of 200 KV.

**2.3.3 Atomic force microscopy (AFM)—**Surface measurements at the nanoscale were evaluated using atomic force microscopy (Nano-R AFM, Pacific Nanotechnology, Santa Clara, CA) in close-contact mode. AFM analyses were conducted using silicon probes (P-MAN-SICC-O, Agilent Technologies, Santa Clara, CA) with dimensions of 1.14 × 0.25 $cm^2$, a nominal force constant of 40 N/m, a nominal resonance frequency of 300 kHz, and tip radii of up to 10 nm. Each AFM analysis was performed over a 730 nm × 730 nm area. Two samples of every group were scanned three times each, under ambient atmosphere. The original data was plane-leveled to remove tilt by applying a numerical second-order correction, and mean values of surface roughness ($S_a$) and peak-to-valley height ($S_z$) were determined using the NanoRule+ software (Pacific Nanotechnology).

**2.3.4 Confocal laser microscopy (CLM)—**Surface roughness at the macro- and micro-scales was evaluated using a confocal laser microscope (Lext, Olympus, Center Valley, PA). Each CLM analysis was performed over a 644 μm × 644 μm area using a scan height step of 50 nm, a 20X objective, and a cutoff wavelength of 100 μm. Two samples of every group were scanned three times each, under ambient atmosphere. Mean values of surface roughness ($S_a$) and peak-to-valley height ($S_z$) were determined.

**2.3.5 X-ray photoelectron spectroscopy (XPS)—**Atomic concentration and chemical bonding information were obtained from the specimen surfaces by X-ray photoelectron spectroscopy (Thermo K-Alpha XPS, Thermo Fisher Scientific, West Palm Beach, FL). The instrument was equipped with a monochromatic Al-Kα X-ray source ($h\nu$ = 1468.6 eV). The XPS analysis chamber was evacuated to a pressure of $5\times10^{-8}$ mbar or lower before collecting XPS spectra. Spectra were collected using an X-ray spot size of 400 μm and pass energy of 100 eV, with 1 eV increments, at a 55° takeoff angle. Two samples of every group were scanned two times each.

**2.3.6 Contact angle measurements—**Contact angle measurements were obtained using a goniometer (CAM 100, KSV, Helsinki, Finland) equipped with a digital camera and image analysis software. Ultra-pure water was used as the wetting liquid, with a drop size of

5 μL. Sessile drop contact angles of the air-water-substrate interface were measured four times in two samples of every group.

**2.3.7 X-ray diffraction (XRD)—**X-ray diffraction analyses were conducted using 1.8 kW Cu Kα radiation, a 1° parallel plate collimator, a ¼ divergence slit, and a 0.04 rad soller slit (X'Pert PRO Alpha-1 diffractometer, PANalytical, Almelo, The Netherlands). Both Bragg-Brentano and θ–2θ parafocusing setups were used for regular and grazing-angle (*i.e.*, 4° take-off angle) analyses, respectively. Two samples of every group were scanned two times each, under ambient atmosphere.

## 2.4 Cell culture model and assays

MG63 cells were obtained from the American Type Culture Collection (Rockville, MD) and were cultured in Dulbecco's modified Eagle medium, containing 10% fetal bovine serum (FBS) and 1% penicillin and streptomycin, at 37°C in an atmosphere of 5% $CO_2$ and 100% humidity. Cells were grown on tissue culture polystyrene (TCPS) or on one of the four types of specimens (PT, NMPT, SLA, NMSLA) at a density of 10,000 cells/$cm^2$. MG63 cells were fed 24 hours after they were plated on the different surfaces and every 48 hours until confluent, as evaluated on the TCPS substrate. At confluence, cells were treated with fresh media for 24 hours and harvested for assays. At harvest, conditioned media were collected and cell layers were washed twice with serum-free media to remove any non-adherent cells, followed by two sequential incubations in 500 μL of 0.25% trypsin for 10 minutes at 37°C to release the cells from the ir substrate. The trypsin reaction was terminated by adding FBS-containing media to the tubes and cells were then centrifuged at 2000 rpm for 15 minutes. The supernatant was decanted, and the cell pellets were resuspended by vortexing in 500 μL of 0.05% Triton-X-100. The cells were then lysed to release cell contents.

Cell proliferation was evaluated by measuring DNA content with a commercially-available kit (QuantiT™ PicoGreen® dsDNA assay, Invitrogen, Carlsbad, CA). Cells were harvested as described above and 50 μL of lysed cell content were diluted with 50 μL of 0.05% Triton-X-100. Fluorescence measurements were obtained using a fluorescent multimode detector (DTX880, Beckman Coulter, Brea, CA) with reference to a standard.

Cell differentiation was evaluated using two markers of osteoblast differentiation: cellular alkaline phosphatase-specific activity [orthophosphoric monoester phosphohydrolase, alkaline; E.C. 3.1.3.1] as an early differentiation marker; and osteocalcin content in the conditioned media as a late differentiation marker. Alkaline phosphatase activity was assayed from the release of *p*-nitrophenol from pnitrophenylphosphate at pH 10.2 as previously described [47]. Activity values were normalized to the protein content, which was detected as colorimetric cuprous cations in biuret reaction (BCA Protein Assay Kit, Pierce Biotechnology Inc., Rockford, IL, USA) at 570 nm (Microplate reader, BioRad Laboratories Inc., Hercules, CA, USA). Osteocalcin levels in the conditioned media were measured using a commercially available radioimmunoassay kit (Human Osteocalcin RIA Kit, Biomedical Technologies, Stoughton, MA), as described previously [48]. Briefly, 50 μL of conditioned media were mixed with [I-125] osteocalcin tracer and human osteocalcin anti-serum (100 μL each), and incubated at 37°C for 2.5 hours. Goat anti-rabbit IgG, polyethylene glycol (100 μL each), and 1 mL of PBS were then added, followed by centrifugation at a minimum of 1500× g for 15 minutes at 4°C. The supernatant was decanted and the pellets were counted for 1 minute in a LS1500 gamma counter (Beckman Coulter, Brea, CA).

The conditioned media were also assayed for protein levels of growth factors and cytokines. Osteoprotegerin (OPG), a cytokine that works as a decoy receptor for "receptor activator for nuclear factor κ B ligand" (RANKL) to inhibit osteoclastogenesis, was measured using

enzyme-linked immunosorbent assay (ELISA) kits (DY805 Osteoprotegerin DuoSet, R&D Systems, Minneapolis, MN). Vascular endothelial growth factor (VEGF), a potent growth factor involved in vasculogenesis and angiogenesis, was also measured using an enzyme-linked immunosorbent assay (ELISA) kit (DY293B VEGF DuoSet, R&D Systems).

### 2.5 Statistical analysis

Data from experiments characterizing the surface properties of the substrates are presented as the mean ± one standard deviation (SD) of all the measurements performed on different samples. Data from experiments examining cell response are presented as mean ± standard error (SE) for six independent cultures. All experiments were repeated at least twice to ensure validity of the observations and results from individual experiments are shown. Data were evaluated by analysis of variance, and significant differences between groups were determined using Bonferroni's modification of Student's t-test. A p value below 0.05 was considered to indicate a statistically-significant difference.

## 3. Results

Scanning electron microscopy (Figs. 2–4) confirmed that a modest temperature oxidation treatment could be used to introduce nanoscale structural features to the Ti surfaces. In this study, the oxidation temperature (*i.e.*, 740°C) and gaseous environment ( *i.e.*, synthetic air) were fixed while the duration of the process was varied. The surfaces of the starting PT samples were relatively smooth on the microscale (CLM $S_a = 0.43 \pm 0.02$ μm), although surface pits, presumably resulting from the PT acid pickling process, were detected (Fig. 2a). After 45 minutes of controlled oxidation (NMPT45), a low density of nanoscale protuberances was observed to have formed on the specimen surfaces (Fig. 2b), with protuberance sizes ranging from about 40 to 200 nm in diameter (Fig. 2e) and about 10 to 150 nm in height. After 90 minutes of modification (NMPT90), the entire surface was homogeneously covered with a relatively high density of nanoscale structures (Fig. 2c), which ranged in size from about 40 to 360 nm in diameter (Fig. 2f) and about 60 to 350 nm in height. Following 180 minutes of modification (NMPT180), the nanostructures coalesced into coarser structures (Fig. 2d) that spanned about 500 to 1000 nm in diameter and about 80 to 500 nm in height. The mass increase of the oxidized samples was also monitored by TG analyses and correlated to changes in surface topography. Indeed, by coupling weight gain measurements to the resulting surface topography, TG analyses may be used to monitor the time required for the generation of a high surface density of nanoscale structures on titanium implants of various geometries.

The NM treatment was also applied to SLA substrates that possessed a greater degree of microscale roughness (CLM $S_a = 3.29 \pm 0.18$ μm) than for the PT specimens. NMSLA samples were generated using the same oxidation conditions as for the NMPT90 samples (*i.e.*, 740°C, 90 min, synthetic flowing air). At low magnifications (Figs. 3a, b), SEM analyses revealed a similar microscale topography for the SLA and NMSLA samples. However, at intermediate and higher magnifications (Figs. 3d, f), NMSLA surfaces were observed to possess a relatively high and uniform density of nanoscale structures.

After verifying that a NM treatment (740°C, 90 min., synthetic flowing air) could be used to introduce a relatively high density of nanoscale structural features to Ti surfaces that were relatively smooth or rough at the microscale, this treatment was applied to Ti specimens for further surface characterization and for use in cell experiments. Cell interactions with four types of specimens were examined: PT (Fig. 4a), NMPT (Fig. 4b), SLA (Fig. 4c) and NMSLA (Fig. 4d). The microscale and nanoscale topography of these samples was measured quantitatively using CLM and AFM, respectively (Table 1). As expected, the mean values of microscale (CLM-derived) roughness and peak-to-valley height obtained for

the PT and NMPT specimens were lower than for the SLA and NMSLA samples. Additionally, the average values of the microscale (CLM-derived) roughness of the nano-modified samples, NMPT and NMSLA, were slightly lower than for the respective controls. The mean nanoscale (AFM-derived) roughness of the NMPT specimens was apparently higher than for the PT controls (Table 1), although little statistical difference in the mean nanoscale roughness could be discerned between the SLA and NMSLA specimens. However, the NMPT and NMSLA surfaces shared noticeably higher (and similar) mean values of nanoscale peak-to-valley height relative to the PT and SLA surfaces. The combined CLM and AFM analyses were consistent with the presence of a relatively high density of nanoscale features on the NMPT and NMSLA specimens with little or no statistical change in the microscale topography.

Water contact angle measurements indicated that all of the samples exhibited relatively hydrophobic behavior (Fig. 5Table 2). The contact angles measured for the SLA and NMSLA samples were significantly larger than for the PT and NMPT samples (Fig. 5Table 2), which was consistent with the enhanced mean values of microscale roughness (CLM-derived $S_a$ values) and microscale peak-to-valley height (CLM-derived $S_z$ values) for the SLA and NMSLA samples (Table 1).

General surveys of the surface chemistry of the different specimens by XPS analyses revealed the presence of appreciable oxygen and titanium. Within statistical error, the concentrations of oxygen and titanium on the PT and NMPT surfaces, and of oxygen and titanium on the SLA and NMSLA surfaces, were similar (Table 3). However, a detectable change in the phase content on the Ti surfaces after the NM treatment was revealed by XRD and TEM analyses (Fig. 5). XRD analyses of the surfaces of the PT and SLA samples yielded major diffraction peaks for α-Ti (ICDD 01-089-3073) and did not yield detectable diffraction peaks for crystalline oxides of titanium (Fig. 5e). The SLA samples also exhibited additional diffraction peaks of modest intensity that were attributed to titanium hydride ($TiH_2$, ICDD 04-008-1386). Both NMPT and NMSLA specimens exhibited relatively intense diffraction peaks for the rutile polymorph of $TiO_2$ (ICDD 01-071-6411). The α-Ti diffraction peaks in the NM-treated samples also appeared to shift to lower two-theta values. TEM analysis of an ion-milled cross-section of the NMPT sample (Fig. 5f) revealed the presence of a compact and conformal oxide layer on the Ti surface. The average thickness of this oxide layer, generated within 90 min at 740°C in air, was about 1.2 μm. Selected area electron diffraction (SAED) analysis (Fig. 5g) of this oxide scale yielded a diffraction pattern that was consistent with the presence of only the rutile polymorph of $TiO_2$ (as had also been revealed by the XRD analyses of NM-treated specimens).

Osteoblasts were sensitive to the surface modifications. The number of MG63 osteoblast cells, as deduced from DNA measurements (Fig. 6a), and the alkaline phosphatase specific activity (Fig. 6b) for the NMPT, SLA, and NMSLA samples were statistically lower than for the PT specimens. This reduction in cell content and ALP activity paralleled an increase in mean nanoscale roughness (NMPT vs. PT) and the microscale roughness (SLA and NMSLA vs. PT). While the levels of osteocalcin, osteoprotegerin, and vascular endothelial growth factor (Figs. 6c–e) measured for the PT and NMPT samples were not noticeably different, statistically-significant increases in the levels of these markers were observed for the SLA specimens, which paralleled the increase in microscale roughness for the SLA specimens relative to the PT and NMPT samples (Table 1). Further statistically significant increases in the osteocalcin, osteoprotegerin, and VEGF levels over the SLA specimens was observed for the NMSLA specimens.

## 4. Discussion

In the present study, a simple, readily-scalable (non-line-of-sight) oxidation-based surface modification process was developed that resulted in the superimposition of a high density of nanoscale structures on Ti substrates (as revealed by SEM and AFM analyses) in the absence or presence of appreciable microscale roughness. This nanoscale modification (NM) treatment did not affect surface chemistry (as revealed by XPS measurements) or wettability (as revealed by water contact angle measurements), and did change surface crystal structure (as revealed by XRD and TEM analyses). Moreover, osteoblast behavior was sensitive to the modified surfaces.

The development of this oxidation-based modification process involved correlation of the changes in surface topography and weight of Ti disks with the duration of oxidation in synthetic air at 740°C. Two types of Ti specimens were examined: pretreated specimens, and large-grit sandblasted and acid-etched specimens. As expected, confocal laser microscopy measurements indicated that the microscale surface roughness of the SLA specimens was significantly enhanced relative to the PT specimens. SEM analyses revealed the formation of nanoscale structures on the specimen surfaces upon oxidation at 740°C for times between 45 and 180 min. With an increase in oxidation time, the surface density and average sizes of nanoscale structures formed on this scale increased. After 90 min, a relatively high density of such structures was observed to have formed uniformly over the specimen surfaces, with the SEM-derived diameters and heights ranging from about 40 to 360 nm and about 60 to 350 nm respectively. It is interesting to note that the nanostructures formed by the present oxidation-based process are not unlike the nanostructures associated with collagen fibrils left by osteoclasts after bone resorption [20, 22]. The average values of the CLM-derived microscale roughness ($S_a$) and the peak-to-valley height ($S_z$) for the nano-modified samples were slightly lower than for the respective controls. At least one contribution to such modest reductions in the average $S_a$ and $S_z$ values was likely to have been the formation of the 1.2 μm-thick oxide scale. AFM measurements revealed a significant increase in the mean nanoscale surface roughness, and mean peak-to-valley height, after exposure of PT samples to this 740°C/90 min oxidation treatment. While a statistically-significant increase in the mean nanoscale roughness could not be detected after exposure of SLA specimens to this 740°C/90 min treatment, a significant increase in the mean peak-to-valley height was detected.

XPS analyses indicated that exposure of the PT and SLA specimens to the 740°C/90 min treatment did not greatly affect the concentration of titanium and oxygen on the surfaces of these specimens, which was not surprising due to the presence of a native titanium oxide layer on both original and modified samples. The water contact angles on the PT and SLA samples also did not appreciably change after the 740°C/90 min oxidation treatment. However, XRD and TEM analyses revealed that this treatment resulted in the formation of a compact and conformal rutile $TiO_2$ scale of about 1.2 microns thickness. Noticeable shifts in the two-theta positions of α-Ti diffraction peaks were also detected in the modified samples, which was consistent with an expansion of the α-Ti lattice associated with the incorporation of oxygen [49–50] (note: the solubility of oxygen in α-Ti at 740°C is 33.3 at% [49]).

A high density of nanoscale structures, as well as the presence of appreciable microscale roughness, affected the proliferation of MG63 cells. The number of MG63 osteoblast cells detected on the nanomodified PT (NMPT) samples was lower than for the starting PT specimens. Similarly, cell numbers on SLA and nanoscale-modified SLA (NMSLA) samples were lower than on the PT specimens. In previous studies, cell proliferation on combined micro-/nano-rough surfaces has been reported to increase when compared to micro-rough surfaces [13, 44]. However, in some of these studies, cell proliferation was

evaluated at very early time points (*i.e.*, two days or less), using assays that tested for cell metabolic activity rather than for proliferation [13]. Although simultaneous and enhanced cell proliferation and differentiation would provide an ideal situation for bone growth and repair, studies have shown that the development of the osteoblast phenotype requires a regulated interrelation between proliferation and differentiation with transcriptionally restricted transitions that mark the end point of proliferation and the onset of differentiation [51–53].

Osteoblast differentiation was greatly enhanced on surfaces that possessed both microscale roughness and a high density of nanoscale features. These results are in agreement with previous studies [12, 41], which have indicated that a combination of nanoscale features and microscale roughness are required to achieve an additive, if not synergistic increase, in osteoblast differentiation. In our study, ALP activity was reduced and osteocalcin production was increased in a surface micro-roughness and nanostructure density dependent manner. Other studies reported larger ALP stained areas [13] and higher ALP activity as well as higher osteocalcin gene expression [14] for osteoblasts grown on micro-/nano-structured surfaces. Differences in ALP activity between the present results and those of other studies could be due to the biphasic nature of ALP, which has been shown to increase at the early stages of osteoblast differentiation followed by a decrease in activity when more mature osteoblasts start producing osteocalcin just before mineralization [54].

The cells growing on the NMSLA surfaces also produced significantly higher levels of the local factor osteoprotegerin, which inhibits osteoclastogenesis, and VEGF, which is a potent angiogenic factor. Taken together with the DNA, ALP, and osteocalcin measurements, these results suggest that the combined superimposition of a high density of nanoscale structures with a surface possessing appreciable micro-/submicro-scale roughness may promote bone formation directly in contact with the surface as well as in the surrounding tissue, thereby improving implant osseointegration.

## 5. Conclusions

A simple and readily-scalable (non-line-of-sight) oxidation-based surface modification process has been developed that superimposes a high density of nanoscale structures on the surfaces of Ti samples without greatly affecting other surface properties (e.g., microscale roughness, hydrophobicity). The nanoscale structures are not unlike the nanoscale topography associated with collagen fibrils left by the osteoclasts after bone resorption. The results suggest that, while the nanostructures alone may regulate osteoblast proliferation, osteoblast differentiation is not appreciably affected in the absence of microscale surface roughness. However, the combination of micro-/submicro-scale surface roughness with a high density of nanoscale structures resulted in an additive, if not synergistic effect, on cell differentiation and local factor production. These results suggest a potential opportunity for faster healing times and improved *in vivo* implant osseointegration through mimicry of bone hierarchical complexity via the combined tailoring of nanoscale and microscale surface features.

## Acknowledgments

This research was supported by USPHS AR052102, and the ITI Foundation. RAGI is partially supported by a fellowship from IFARHU-SENACYT. Support for the work of TM, YC, and KHS was provided by the Air Force Office of Scientific Research (Dr. Charles Lee, program manager). The PT and SLA disks were provided by Institut Straumann AG.

## References


1. Kieswetter K, Schwartz Z, Dean DD, Boyan BD. The role of implant surface characteristics in the healing of bone. Crit Rev Oral Biol Medicine. 1996; 7(4):329–345.
2. Schwartz Z, Boyan BD. Underlying mechanisms at the bone-biomaterial interface. J Cell Biochem. 1994; 56:340–347. [PubMed: 7876327]
3. Martin JY, Schwartz Z, Hummert TW, Schraub DM, Simpson J, Lankford J, et al. Effect of titanium surface-roughness on proliferation, differentiation, and protein-synthesis of human osteoblast-like cells (mg63). J Biomed Mater Res. 1995; 29(3):389–401. [PubMed: 7542245]
4. Boyan BD, Bonewald LF, Paschalis EP, Lohmann CH, Rosser J, Cochran DL, et al. Osteoblast-mediated mineral deposition in culture is dependent on surface microtopography. Calcif Tissue Int. 2002; 71(6):519–529. [PubMed: 12232675]
5. Sul YT, Johansson C, Wennerberg P, Cho LR, Chang BS, Albrektsson P. Optimum surface properties of oxidized implants for reinforcement of osseointegration: Surface chemistry, oxide thickness, porosity, roughness, and crystal structure. Int J Oral Maxillofac Implants. 2005; 20(3): 349–359. [PubMed: 15973946]
6. Buser D, Broggini N, Wieland M, Schenk RK, Denzer AJ, Cochran DL, et al. Enhanced bone apposition to a chemically modified sla titanium surface. J Dent Res. 2004; 83(7):529–533. [PubMed: 15218041]
7. Liu X, Lim JY, Donahue HJ, Dhurjati R, Mastro AM, Vogler EA. Influence of substratum surface chemistry/energy and topography on the human fetal osteoblastic cell line hfob 1.19: Phenotypic and genotypic responses observed in vitro. Biomaterials. 2007; 28(31):4535–4550. [PubMed: 17644175]
8. Rupp F, Scheideler L, Olshanska N, deWild M, Wieland M, Geis-Gerstorfer J. Enhancing surface free energy and hydrophilicity through chemical modification of microstructured titanium implant surfaces. J Biomed Mater Res. 2006; 76A:323–334.
9. Zhao G, Schwartz Z, Wieland M, Rupp F, Geis-Gerstorfer J, Cochran DL, et al. High surface energy enhances cell response to titanium substrate microstructure. J Biomed Mater Res. 2005; 74A:49–58.
10. Schwartz Z, Raz P, Zhao G, Barak Y, Tauber M, Yao H, et al. Effect of micrometer-scale roughness of the surface of ti6al4v pedicle screws in vitro and in vivo. J Bone Joint Surg Am. 2008; 90A(11):2485–2498. [PubMed: 18978418]
11. Att W, Tsukimura N, Suzuki T, Ogawa T. Effect of supramicron roughness characteristics produceed by 1-and 2-step acid etching on the osseointegration capability of titanium. Int J Oral Maxillofac Implants. 2007; 22(5):719–728. [PubMed: 17974105]
12. Zhao G, Zinger O, Schwartz Z, Wieland M, Landolt D, Boyan BD. Osteoblast-like cells are sensitive to submicron-scale surface structure. Clin Oral Implants Res. 2006; 17(3):258–264. [PubMed: 16672020]
13. Kubo K, Tsukimura N, Iwasa F, Ueno T, Saruwatari L, Aita H, et al. Cellular behavior on tio2 nanonodular structures in a micro-to-nanoscale hierarchy model. Biomaterials. 2009; 30(29): 5319–5329. [PubMed: 19589591]
14. Mendonca G, Mendonca DBS, Aragao FJL, Cooper LF. The combination of micron and nanotopography by h2so4/h2o2 treatment and its effects on osteoblast-specific gene expression of hmscs. J Biomed Mater Res. 2010; 94A(1):169–179.
15. Schwartz Z, Lohmann CH, Wieland M, Cochran DL, Dean DD, Textor M, et al. Osteoblast proliferation and differentiation on dentin slices are modulated by pretreatment of the surface with tetracycline or osteoclasts. J Periodontol. 2000; 71(4):586–597. [PubMed: 10807123]
16. Mulari MTK, Qu Q, Harkonen PL, Vaananen HK. Osteoblast-like cells complete osteoclastic bone resorption and form new mineralized bone matrix in vitro. Calcif Tissue Int. 2004; 75(3):253–261. [PubMed: 15148559]
17. Mori S, Burr DB. Increased intracortical remodeling following fatigue damage. Bone. 1993; 14(2): 103–109. [PubMed: 8334026]
18. Baron R, Neff L, Louvard D, Courtoy PJ. Cell-mediated extracellular acidification and bone-resorption - evidence for a low ph in resorbing lacunae and localization of a 100-kd lysosomal

membrane-protein at the osteoclast ruffled border. J Cell Biol. 1985; 101(6):2210–2222. [PubMed: 3905822]

19. Chambers TJ, Revell PA, Fuller K, Athanasou NA. Resorption of bone by isolated rabbit osteoclasts. J Cell Sci. 1984; 66(MAR):383–399. [PubMed: 6746762]
20. Rho JY, Kuhn-Spearing L, Zioupos P. Mechanical properties and the hierarchical structure of bone. Med Eng Phys. 1998; 20(2):92–102. [PubMed: 9679227]
21. Boyde A, Ali NN, Jones SJ. Optical and scanning electron-microscopy in the single osteoclast resorption assay. Scan Electron Microsc. 1985:1259–1271. [PubMed: 2416039]
22. Boyan BD, Schwartz Z, Lohmann CH, Sylvia VL, Cochran DL, Dean DD, et al. Pretreatment of bone with osteoclasts affects phenotypic expression of osteoblast-like cells. J Orthop Res. 2003; 21(4):638–647. [PubMed: 12798063]
23. Teitelbaum SL, Ross FP. Genetic regulation of osteoclast development and function. Nat Rev Genet. 2003; 4(8):638–649. [PubMed: 12897775]
24. Kieswetter K, Schwartz Z, Hummert TW, Cochran DL, Simpson J, Dean DD, et al. Surface roughness modulates the local production of growth factors and cytokines by osteoblast-like mg-63 cells. J Biomed Mater Res. 1996; 32(1):55–63. [PubMed: 8864873]
25. Raines AL, Olivares-Navarrete R, Wieland M, Cochran DL, Schwartz Z, Boyan BD. Regulation of angiogenesis during osseointegration by titanium surface microstructure and energy. Biomaterials. 2010; 31(18):4909–4917. [PubMed: 20356623]
26. Buser D, Schenk RK, Steinemann S, Fiorellini JP, Fox CH, Stich H. Influence of surface characteristics on bone integration of titanium implants - a histomorphometric study in miniature pigs. J Biomed Mater Res. 1991; 25(7):889–902. [PubMed: 1918105]
27. Cochran DL, Schenk RK, Lussi A, Higginbottom FL, Buser D. Bone response to unloaded and loaded titanium implants with a sandblasted and acid-etched surface: A histometric study in the canine mandible. J Biomed Mater Res. 1998; 40(1):1–11. [PubMed: 9511093]
28. Cochran DL. A comparison of endosseous dental implant surfaces. J Periodontol. 1999; 70(12): 1523–1539. [PubMed: 10632528]
29. Cochran DL, Buser D, ten Bruggenkate CM, Weingart D, Taylor TM, Bernard JP, et al. The use of reduced healing times on iti (r) implants with a sandblasted and acid-etched (sla) surface: Early results from clinical trials on iti (r) sla implants. Clin Oral Implants Res. 2002; 13(2):144–153. [PubMed: 11952734]
30. Lipski AM, Pino CJ, Haselton FR, Chen IW, Shastri VP. The effect of silica nanoparticle-modified surfaces on cell morphology, cytoskeletal organization and function. Biomaterials. 2008; 29(28): 3836–3846. [PubMed: 18606447]
31. Curtis ASG, Gadegaard N, Dalby MJ, Riehle MO, Wilkinson CDW, Aitchison G. Cells react to nanoscale order and symmetry in their surroundings. IEEE Trans Nanobioscience. 2004; 3(1):61–65. [PubMed: 15382646]
32. Riehle MO, Dalby MJ, Johnstone H, MacIntosh A, Affrossman S. Cell behaviour of rat calvaria bone cells on surfaces with random nanometric features. Mater Sci Eng C Biomimetic Supramol Syst. 2003; 23(3):337–340.
33. Ward BC, Webster TJ. Increased functions of osteoblasts on nanophase metals. Mater Sci Eng C Biomimetic Supramol Syst. 2007; 27(3):575–578.
34. Biggs MJP, Richards RG, Gadegaard N, McMurray RJ, Affrossman S, Wilkinson CDW, et al. Interactions with nanoscale topography: Adhesion quantification and signal transduction in cells of osteogenic and multipotent lineage. Journal of Biomedical Materials Research Part A. 2009; 91A(1):195–208. [PubMed: 18814275]
35. Palin E, Liu HN, Webster TJ. Mimicking the nanofeatures of bone increases bone-forming cell adhesion and proliferation. Nanotechnology. 2005; 16(9):1828–1835.
36. Dalby MJ, McCloy D, Robertson M, Wilkinson CDW, Oreffo ROC. Osteoprogenitor response to defined topographies with nanoscale depths. Biomaterials. 2006; 27(8):1306–1315. [PubMed: 16143393]
37. Webster TJ, Ergun C, Doremus RH, Siegel RW, Bizios R. Enhanced functions of osteoblasts on nanophase ceramics. Biomaterials. 2000; 21(17):1803–1810. [PubMed: 10905463]

38. Webster TJ, Ejiofor JU. Increased osteoblast adhesion on nanophase metals: Ti, ti6al4v, and cocrmo. Biomaterials. 2004; 25(19):4731–4739. [PubMed: 15120519]
39. Washburn NR, Yamada KM, Simon CG, Kennedy SB, Amis EJ. High-throughput investigation of osteoblast response to polymer crystallinity: Influence of nanometer-scale roughness on proliferation. Biomaterials. 2004; 25(7–8):1215–1224. [PubMed: 14643595]
40. Cai KY, Bossert J, Jandt KD. Does the nanometre scale topography of titanium influence protein adsorption and cell proliferation? Colloids Surf B Biointerfaces. 2006; 49(2):136–144. [PubMed: 16621470]
41. Zinger O, Zhao G, Schwartz Z, Simpson J, Wieland M, Landolt D, et al. Differential regulation of osteoblasts by substrate microstructural features. Biomaterials. 2005; 26(14):1837–1847. [PubMed: 15576158]
42. Guo J, Padilla RJ, Ambrose W, De Kok IJ, Cooper LF. The effect of hydrofluoric acid treatment of tio2 grit blasted titanium implants on adherent osteoblast gene expression in vitro and in vivo. Biomaterials. 2007; 28(36):5418–5425. [PubMed: 17868850]
43. Mendonca G, Mendonca DBS, Simoes LGP, Araujo AL, Leite ER, Duarte WR, et al. The effects of implant surface nanoscale features on osteoblast-specific gene expression. Biomaterials. 2009; 30(25):4053–4062. [PubMed: 19464052]
44. Zhao L, Mei S, Chu PK, Zhang Y, Wu Z. The influence of hierarchical hybrid micro/nano-textured titanium surface with titania nanotubes on osteoblast functions. Biomaterials. 2010; 31(19):5072–5082. [PubMed: 20362328]
45. Mendes VC, Moineddin R, Davies JE. The effect of discrete calcium phosphate nanocrystals on bone-bonding to titanium surfaces. Biomaterials. 2007; 28(32):4748–4755. [PubMed: 17697709]
46. Gittens, RA.; Sandhage, KH.; Schwartz, Z.; Tannenbaum, R.; Boyan, BD. Surface modification under controlled oxidative environment. U.S. Patent Application No. 61/299,433. 2010.
47. Bretaudiere JP, Spillman T. Alkaline phosphatases. Methods of Enzymatic Analysis, Verlag Chemica. 1984:75–92.
48. Boyan BD, Batzer R, Kieswetter K, Liu Y, Cochran DL, Szmuckler-Moncler S, et al. Titanium surface roughness alters responsiveness of mg63 osteoblast-like cells to 1 alpha,25-(oh)(2)d-3. J Biomed Mater Res. 1998; 39(1):77–85. [PubMed: 9429099]
49. Murray, JL.; Wriedt, HA. Phase diagrams of binary titanium alloys. Metals Park, OH: ASM International; 1987.
50. Unnam J, Clark RK. Oxidation of commercial purity titanium. Oxid Met. 1986; 26(3–4):231–252.
51. Lian JB, Stein GS, Bortell R, Owen TA. Phenotype suppression - a postulated molecular mechanism for mediating the relationship of proliferation and differentiation by fos/jun interactions at ap-1 sites in steroid responsive promoter elements of tissue-specific genes. J Cell Biochem. 1991; 45(1):9–14. [PubMed: 1900844]
52. Stein GS, Lian JB. Molecular mechanisms mediating proliferation/differentiation interrelationships during progressive development of the osteoblast phenotype. Endocr Rev. 1993; 14(4):424–442. [PubMed: 8223340]
53. Stein GS, Lian JB, Stein JL, VanWijnen AJ, Montecino M. Transcriptional control of osteoblast growth and differentiation. Physiol Rev. 1996; 76(2):593–629. [PubMed: 8618964]
54. Lian JB, Stein GS. Concepts of osteoblast growth and differentiation - basis for modulation of bone cell-development and tissue formation. Crit Rev Oral Biol Medicine. 1992; 3(3):269–305.

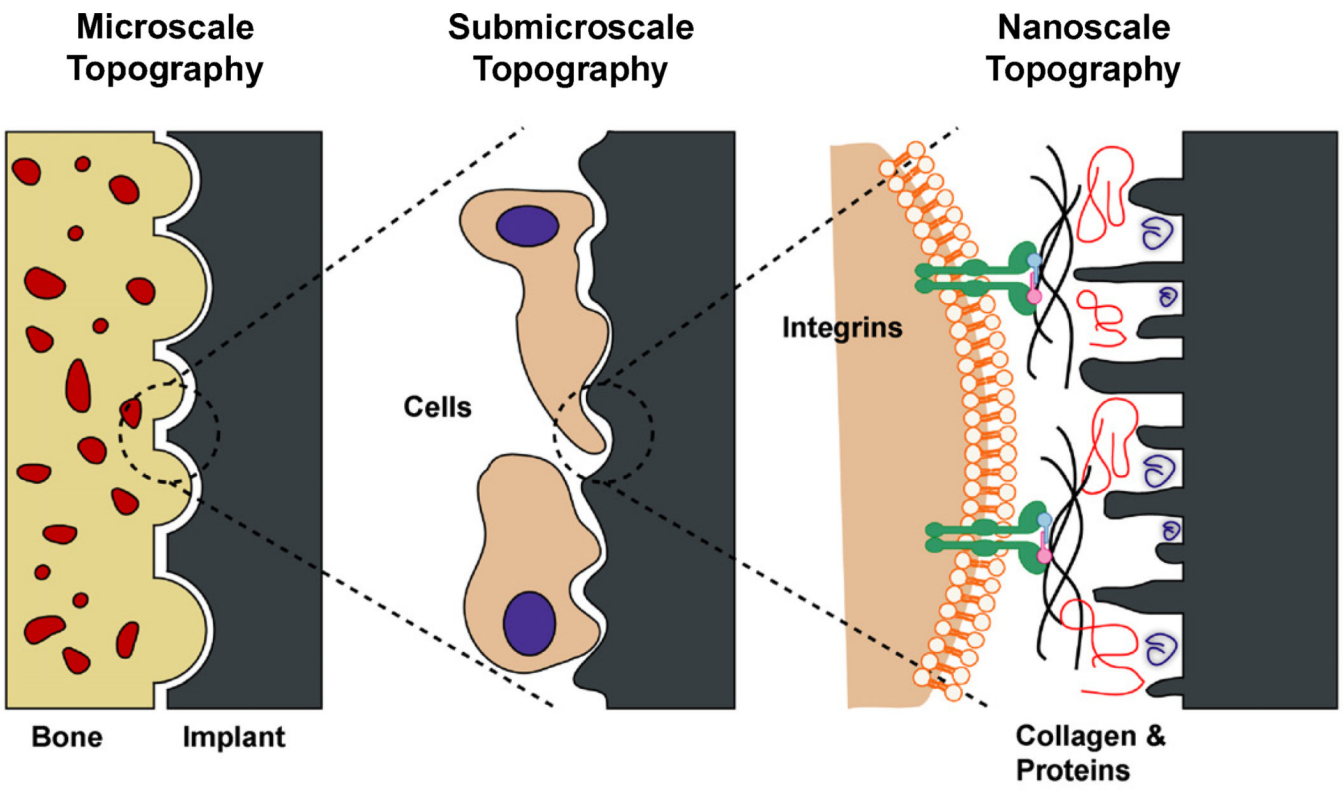


**Figure 1.**
Schematic of the interactions between bone and the implant surface at different topographical scales.

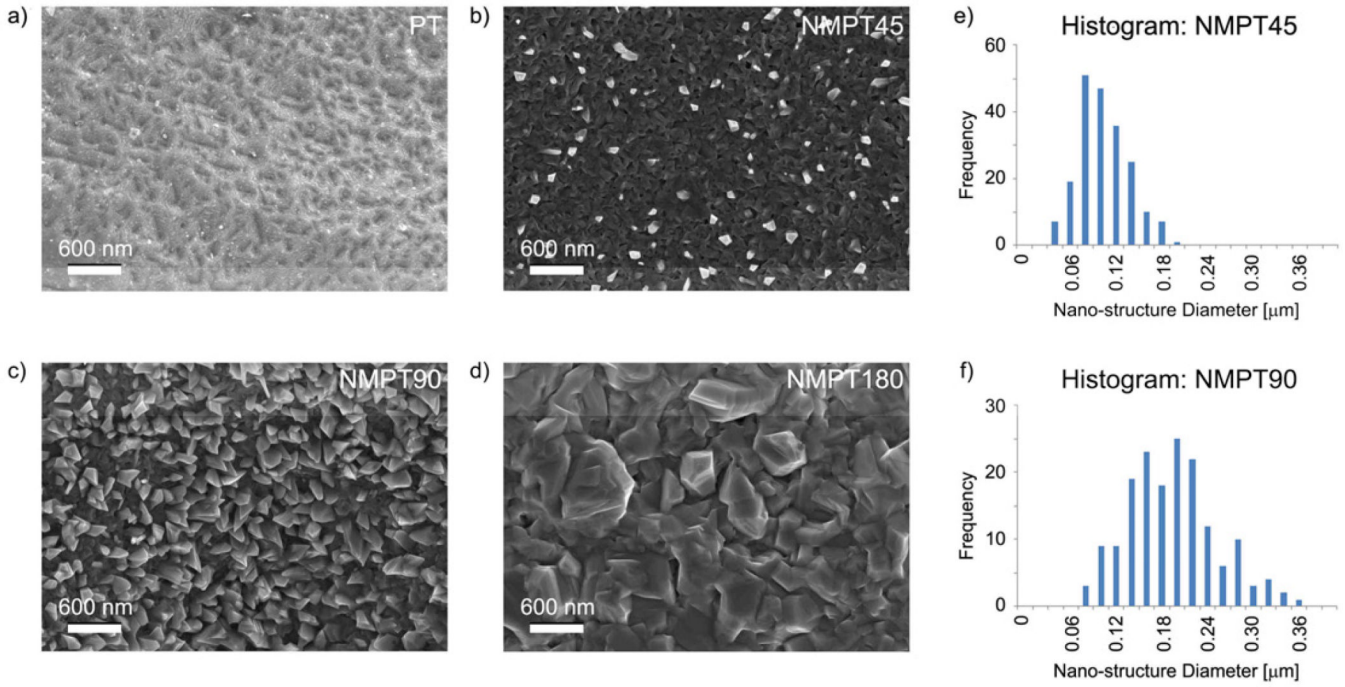


**Figure 2.**

NM-treatment of (a) PT surfaces via oxidation in flowing synthetic air (21% $O_2$, 79% $N_2$) at 740°C for times of: (b) 45 minutes; (c) 90 minutes; (d) 180 minutes. The modification process introduced: (b) nanoscale protuberances with low surface coverage after 45 minutes; (c) a relatively high density of nanostructures after 90 minutes; and (d) coarse structures after 180 minutes. These SEM images are representative of the entire PT Ti disk surfaces. (e, f) Image analyses of SEM images revealing the distribution of diameters of the nanoscale structures formed after 45 minutes and 90 minutes, respectively.

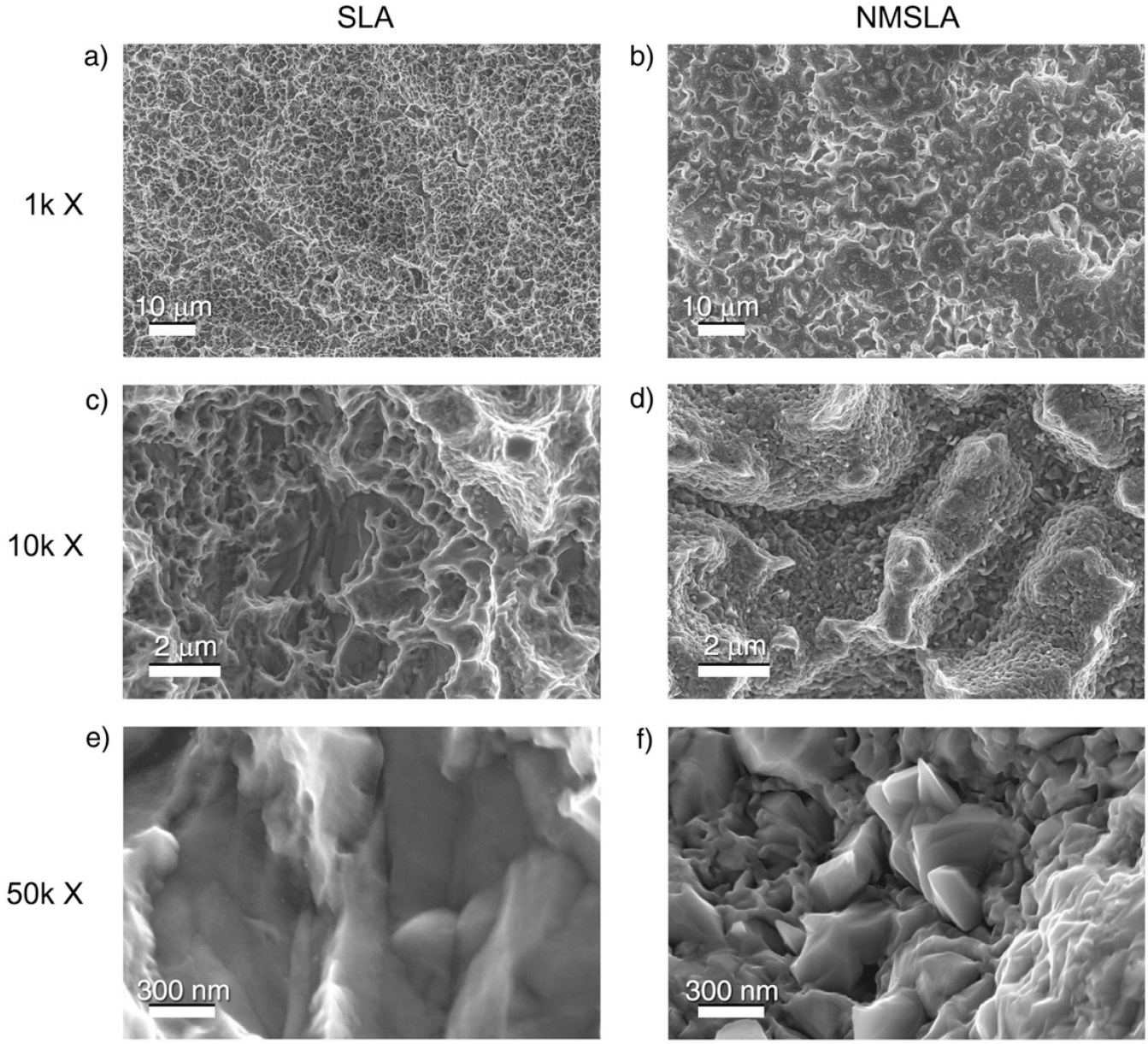


**Figure 3.**
SEM images of starting SLA samples (a, c, e), and of NMSLA samples (b, d, f) generated via oxidation in flowing synthetic air at 740°C for 90 minutes. These images indicate that the NM process yielded a relatively high density of nanoscale structures over the entire specimen surface and did not appreciably affect the overall microscale roughness of the SLA surface.

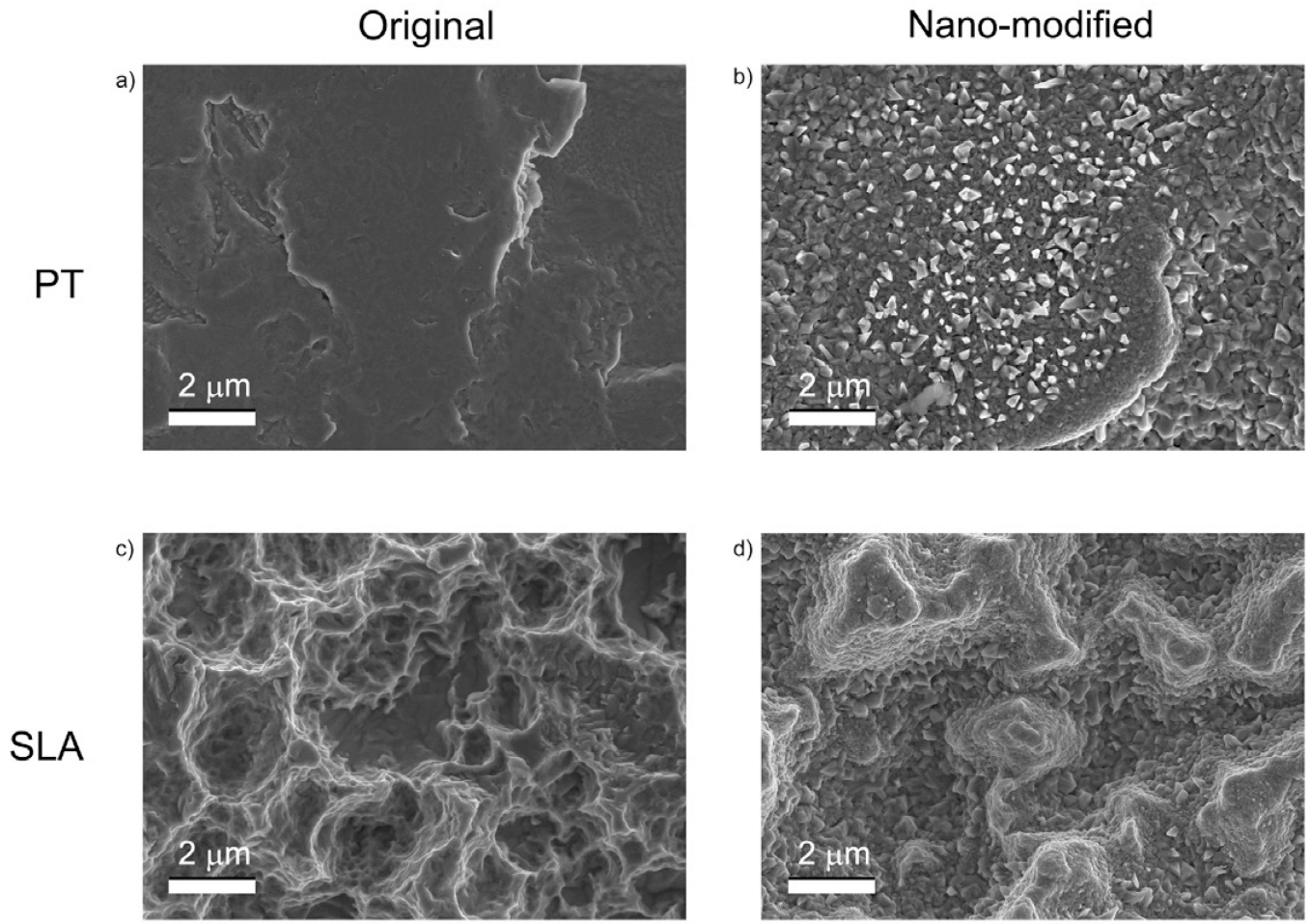


**Figure 4.**
SEM images of the surfaced of (a) PT, (b) NMPT, (c) SLA, and (d) NMSLA samples used for further surface characterization and for cell experiments. The NM treatment consisted of oxidation in flowing synthetic air for 90 min at 740°C.

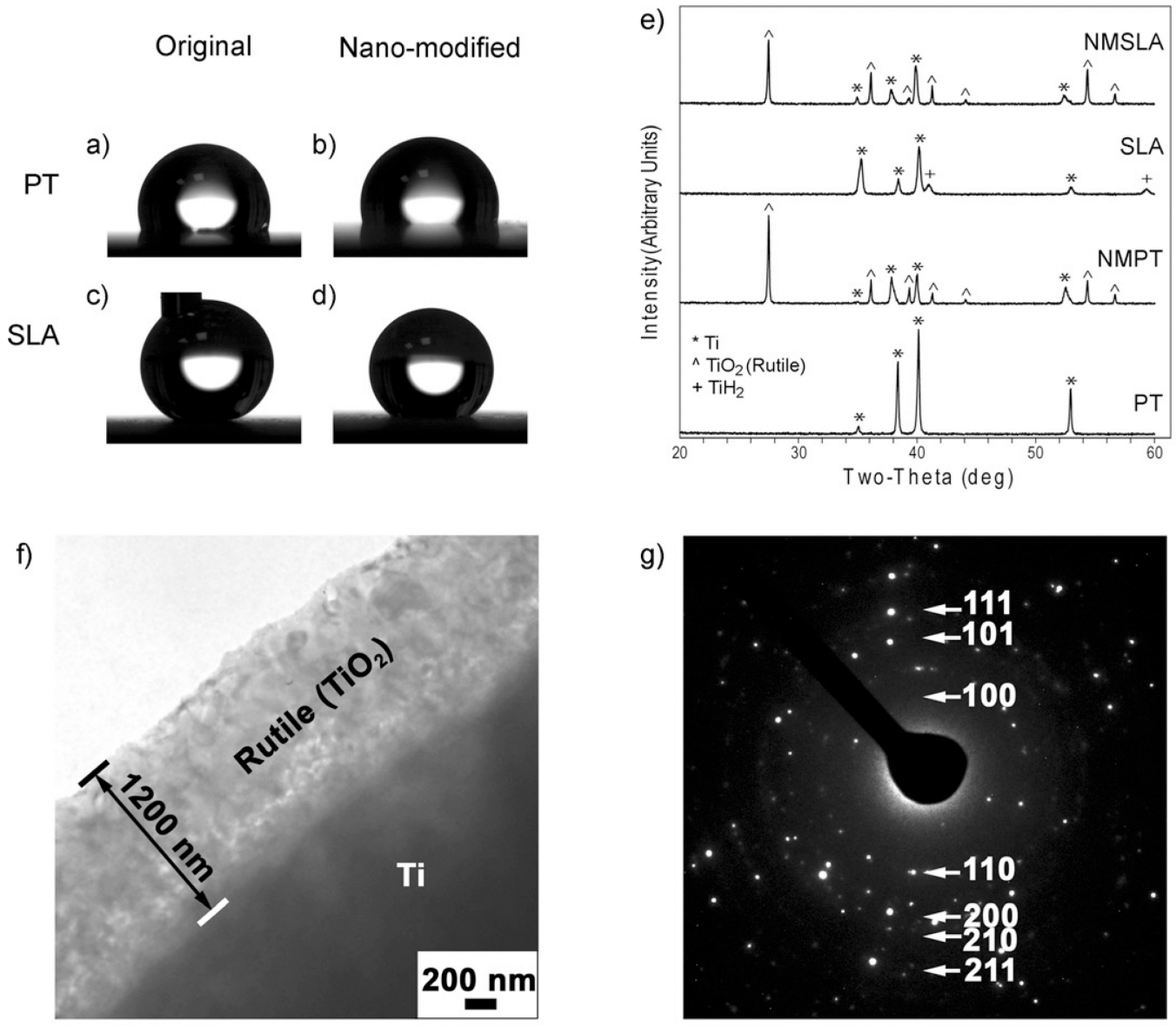


**Figure 5.**

Surface characterization data of the NM-treated samples, which were oxidized in flowing synthetic air for 90 min at 740°C, and their controls. (a–d) Optical images of water contact angles on PT, SLA, NMPT, and NMSLA surfaces. The contact angles measured for PT and NMPT samples were similar and smaller than for the SLA and NMSLA samples. (e) X-ray diffraction (XRD) patterns obtained from PT, SLA, NMPT, and NMSLA samples. (f) TEM image of an ion-milled cross-section of a NMPT specimen revealing the compact and conformal oxide layer formed after NM treatment. The average thickness of this oxide scale was 1.2 μm. (g) Selective area electron diffraction pattern obtained from the oxide scale, which was consistent with pure rutile $TiO_2$.

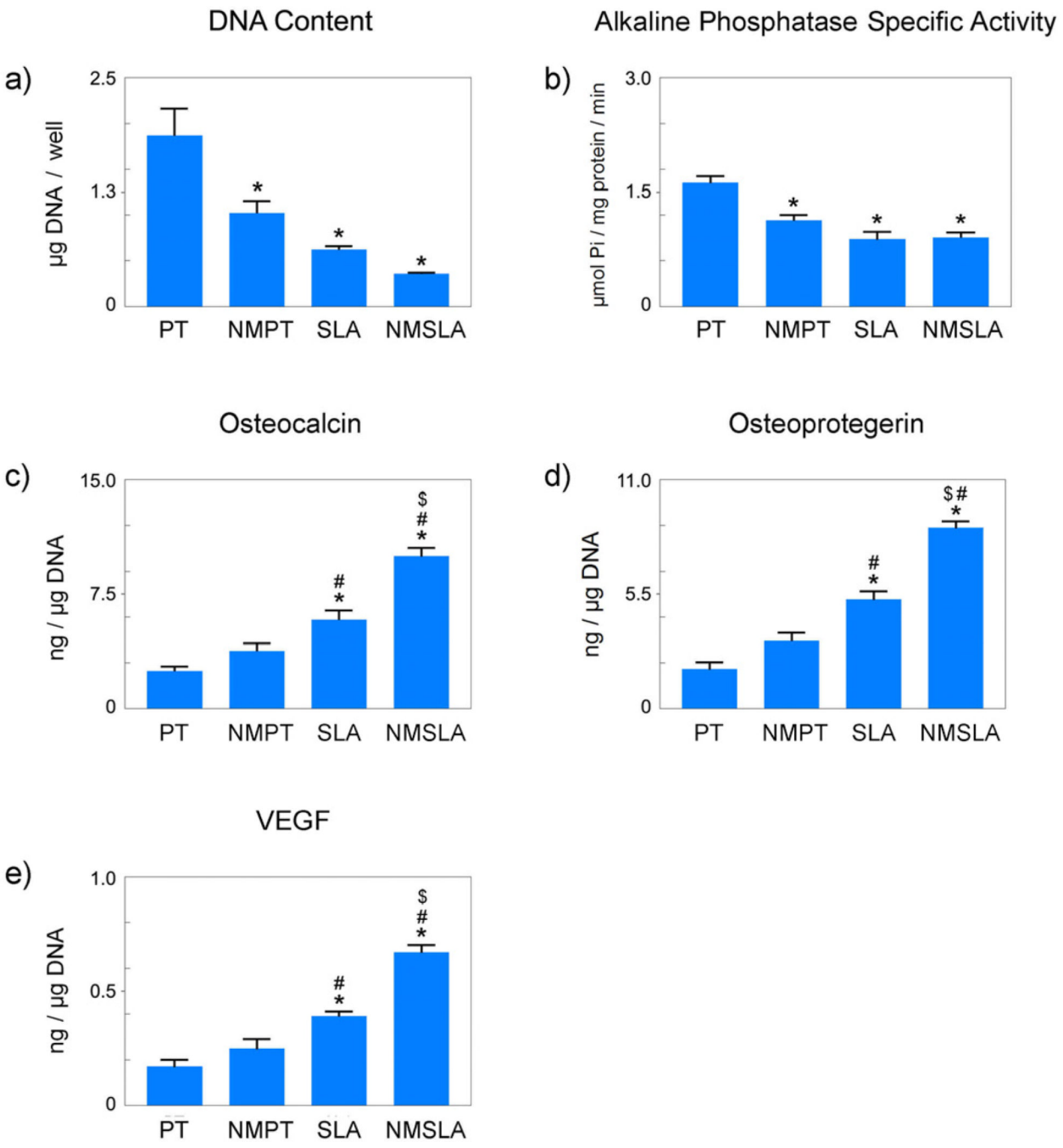


**Figure 6.**

Effects of nanoscale surface features and microscale surface roughness on osteoblast differentiation. MG63 cells were plated on PT, NMPT, SLA, and NMSLA surfaces and grown to confluence. The NM treatment consisted of oxidation in flowing synthetic air for 90 min at 740°C. At confluence, (a) DNA content, ( b) ALP specific activity, (c) OCN, (d) OPG, and (e) VEGF levels were measured. Data represented are the mean ± SE of six independent samples. * refers to a statistically-significant p value below 0.05 vs. PT; # refers to a statistically-significant p value below 0.05 vs. NMPT; $ refers to a statistically-significant p value below 0.05 vs. SLA.

**Table 1**

Mean ± one standard deviation (SD) values of roughness ($S_a$) and peak-to-valley height ($S_z$) of the different titanium surfaces examined using atomic force microscopy (AFM) and confocal laser microscopy (CLM).

| Sample | AFM Mean Roughness ($S_a$) ± 1 SD [nm] | AFM Mean Peak-to-Valley Height ($S_z$) ± 1 SD [nm] | CLM Mean Roughness ($S_a$) ± 1 SD [μm] | CLM Mean Peak-to-Valley Height ($S_z$) ± 1 SD [μm] |
|---|---|---|---|---|
| PT | ---* | 58 ± 41 | 0.43 ± 0.02 | 7.99 ± 1.67 |
| NMPT | 16 ± 8 | 142 ± 69 | 0.37 ± 0.01 | 5.58 ± 0.35 |
| SLA | 14 ± 6 | 50 ± 22 | 3.29 ± 0.18 | 42.01 ± 4.02 |
| NMSLA | 18 ± 3 | 141 ± 80 | 2.80 ± 0.06 | 36.57 ± 2.00 |

*The mean roughness value was below the 10 nm detection limit of the AFM tip.

## Table 2

Mean values of NMPT/PT and NMSLA/SLA O and Ti concentration ratios ± one standard deviation (SD) as determined by x-ray photoelectron spectroscopy (XPS).

| Sample | Mean Ratios of Elemental Concentrations ± 1 SD | |
|---|---|---|
| | O | Ti |
| NMPT/PT | 0.97 ± 0.23 | 0.89 ± 0.20 |
| NMSLA/SLA | 1.24 ± 0.07 | 1.29 ± 0.13 |

## Table 3

Mean values of water contact angle ± one standard deviation (SD).

| Sample | Contact Angle [° ± S.D.] |
|---|---|
| PT | 92 ± 1 |
| NMPT | 101 ± 0 |
| SLA | 157 ± 3 |
| NMSLA | 142 ± 1 |